Enantiodetection via two-dimensional spectroscopy: Extending the methodology to general experimental conditions

Mao-Rui Cai [1], Chong Ye,[2] Yong Li [3,*] and Hui Dong[1,†]

[1]*Graduate School of China Academy of Engineering Physics, Beijing 100193, China*
[2]*Beijing Key Laboratory of Nanophotonics and Ultrafine Optoelectronic Systems, School of Physics, Beijing Institute of Technology, Beijing 100081, China*
[3]*Center for Theoretical Physics and School of Physics and Optoelectronic Engineering, Hainan University, Haikou 570228, China*

Developing effective methods to measure the enantiomeric excess of chiral mixtures is one of the major topics in chiral molecular research but remains challenging. An enantiodetection method via two-dimensional (2D) spectroscopy based on a four-level model containing a cyclic three-level system (CTLS) of chiral molecules was recently proposed and demonstrated, but with a strict condition of one-photon resonance (where three driving fields are exactly resonantly coupled to the three electric dipole transitions) in the CTLS and narrow-band probe-pulse assumption. Here, we extend the 2D spectroscopy method to more general experimental conditions, with three-photon resonance (where the sum of the two smaller frequencies among the three driving fields equals the third one) and a broadband probe pulse. Our method remains effective on enantiodetection with the help of experimental techniques such as the chop-detection method, which is used to eliminate the influence of the other redundant levels that exist in the real system of chiral molecules. Under these more general conditions, the enantiomeric excess of the chiral mixture is estimated by taking an easily available standard sample (usually the racemic mixture) as the reference.

I. INTRODUCTION

Chiral molecules have two species, i.e., enantiomers, which are mirror images of each other. Enantiomers have almost the same physical properties, e.g., energy level structures but act disparately in their biological activities and chemical interaction [1], leading to successive interest in the investigation of enantioseparation [2–10], enantioconversion [11–16], and enantiodetection [17–28]. Enantiomers often have subtle differences in their optical activities, which is an exception to their identical physical properties [17–19]. This makes it possible to detect the enantiomeric excess of a chiral mixture optically. However, traditional spectroscopic methods, such as circular dichroism [17,18] and Raman optical activity [19], typically suffer from a weak signal originating from magnetic dipole or electric quadrupole interactions.

In recent years, new spectroscopic methods of enantiodetection taking advantage of the strong electric dipole coupling have been investigated theoretically [26,27,29,30] and experimentally [22–25], benefiting from the study of the cyclic three-level system (CTLS) of chiral molecules [31–36], in which three electromagnetic driving fields are coupled to three electric dipole transitions among the three energy levels of the chiral molecules. Typically, most of these methods require a standard enantiopure sample for the reference [22–25]. However, acquiring the enantiopure sample itself remains challenging for most chiral molecules. We recently proposed enantiodetection methods that do not require an enantiopure

sample using either one-dimensional (1D) or two-dimensional (2D) spectroscopy [26,27]. In the method using the 2D spectroscopy, three probe pulses are applied in a sequence to detect the chirality-dependent energy shifts engineered by the three electromagnetic driving fields in the CTLS [26,27]. Signals from different enantiomers are naturally categorized in the 2D spectrum because any two diagonal peaks corresponding to different enantiomers have no off-diagonal correspondence [27,37]. This feature of the 2D spectroscopy provides an advantage over the 1D case, where additional procedures are required for peak categorization.

We have demonstrated the effectiveness of our enantiodetection method [27] via 2D spectroscopy under ideal experimental conditions, e.g., one-photon resonance [38] of the driving fields in the CTLS and the use of narrow-band probe pulses for single-transition excitation. However, in the case of one-photon resonance, all three driving fields are resonantly coupled to the three electric dipole transitions without detuning. This demands a full understanding of the energy levels of the investigated chiral molecules, limiting the universal application of this method to enantiodetection. Moreover, generating narrow-band pulses covering only one transition is challenging. In existing experiments with 2D spectroscopy, the bandwidth of the probe pulses is usually broad, and multiple transitions from the ground level to the excited levels can be induced [39–41], which poses a challenge for this method on enantiodetection, as induced multiple transitions may affect the ability of the 2D spectroscopy to distinguish between different enantiomers.

In this paper we extend the 2D-spectroscopy-based enantiodetection method to more general cases. Specifically, we
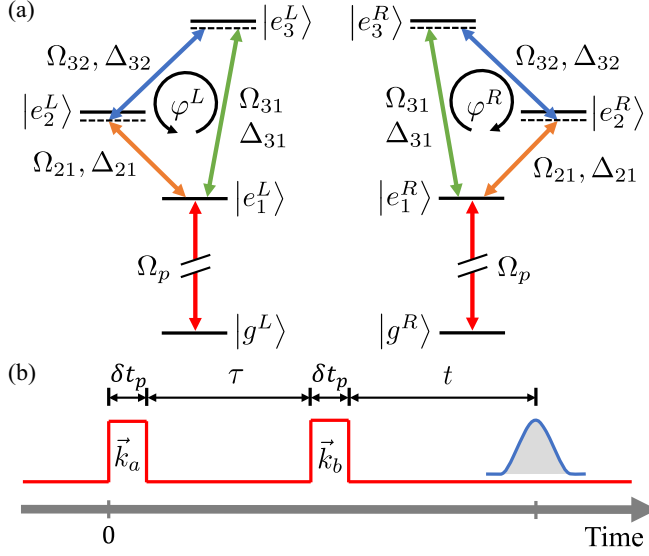
FIG. 1. (a) The basic model with a CTLS and the ground level of the chiral molecules. In the subsystem, three driving fields are nearly resonantly coupled to the three transitions $|e_j^\alpha\rangle \leftrightarrow |e_l^\alpha\rangle$ with Rabi frequencies Ω_{jl}, detunings Δ_{jl}, and overall phases φ^α. The probe pulses $\vec{k}_p$ ($p = a, b$) induce only the transition $|g^\alpha\rangle \leftrightarrow |e_1^\alpha\rangle$ with Rabi frequencies Ω_p. (b) The probe pulse sequence. Two probe pulses $\vec{k}_a$ and $\vec{k}_b$, denoted by the rectangles, are separated by an interval τ. The signal denoted by the curve is detected at time t after the second probe pulse $\vec{k}_b$. The two probe pulses have the same duration δt_p.

demonstrate that different enantiomers can still be distinguished by their separate chirality-dependent peaks in the 2D spectrum even under three-photon resonance [26,31] and with the use of broadband probe pulses. Under three-photon resonance, the three driving fields are coupled to the corresponding transitions with detunings, and the sum of the two smaller frequencies of the driving fields equals the third one. This condition is preferred in experiments, compared to the one-photon resonance, when one has only rough knowledge of the enantiomers of interest. We demonstrate that under three-photon resonance, the enantiomeric excess of a chiral mixture is estimated by taking the easy-to-get racemic mixture as the reference. In more general situations where transitions from the ground state to all three working excited states, as well as other redundant states, are induced by broadband probe pulses, we prove that these induced multiple transitions do not affect the enantiodetection via the 2D spectrum. To achieve enantiodetection in these general situations, we adopt advanced experimental techniques, i.e., the chop detection [39–41] and truncation method to eliminate the influence of the other redundant levels.

II. THREE-PHOTON RESONANCE

The CTLS, in which three electric dipole transitions among the three energy levels are all allowed, is forbidden in natural atoms but universally exists in chiral molecules whose symmetry is naturally broken. With this fact, we propose the basic model of this paper in Fig. 1(a). The model consists of a CTLS with three excited states $|e_j^\alpha\rangle$ ($j = 1, 2, 3$) and a ground state

$|g^\alpha\rangle$ for left-handed ($\alpha = L$) and right-handed ($\alpha = R$) chiral molecules [30,42,43]. Three constant electromagnetic driving fields (typically in the microwave region) with central frequencies ν_{jl} ($j > l$) are applied to couple the corresponding electric dipole transitions $|e_j^\alpha\rangle \leftrightarrow |e_l^\alpha\rangle$ with detunings $\Delta_{jl} = \omega_j - \omega_l - \nu_{jl}$ under three-photon resonance ($\nu_{21} + \nu_{32} = \nu_{31}$, i.e., $\Delta_{21} + \Delta_{32} = \Delta_{31}$). Here, ω_j are eigenenergies of states $|e_j\rangle$ with ground-state energy $\omega_0 = 0$. The Hamiltonian of the system is given in the interaction picture with respect to $H'_\alpha = \sum_j \omega'_j |e_j^\alpha\rangle\langle e_j^\alpha|$ as ($\hbar = 1$, $\omega'_1 = \omega_1$, $\omega'_2 = \omega_1 + \nu_{21}$, and $\omega'_3 = \omega_1 + \nu_{31}$)

$$V_{\text{cyc}}^\alpha = \Delta_{21} |e_2^\alpha\rangle\langle e_2^\alpha| + \Delta_{31} |e_3^\alpha\rangle\langle e_3^\alpha| + (\Omega_{21} |e_2^\alpha\rangle\langle e_1^\alpha| + \Omega_{31} |e_3^\alpha\rangle\langle e_1^\alpha| + \Omega_{32} e^{i\varphi^\alpha} |e_3^\alpha\rangle\langle e_2^\alpha| + \text{H.c.}). \quad (1)$$

Here, Ω_{jl} are Rabi frequencies, and φ^α is the effective overall phase, which differs by π for the different enantiomers [31,32], i.e., $\varphi^R = \varphi^L + \pi$.

In the proposed model, two pulses with wave vector $\vec{k}_p$ ($p = a, b$), short duration δt_p, and interval τ are applied to probe the chirality-dependent shifts induced by the driving fields [26]. The pulse sequence is illustrated in Fig. 1(b). An assumption is made that the probe pulses induce only the transition $|g^\alpha\rangle \leftrightarrow |e_1^\alpha\rangle$ with central frequency $\nu_p = \omega_1$ and narrow bandwidth $\delta\nu_p \ll \{\omega_{21}, \omega_{31}\}$, where $\omega_{ij} = |\omega_i - \omega_j|$. The Hamiltonian within the short duration of the probe pulse is given in the interaction picture with respect to $H_0^\alpha = \sum_j \omega_j |e_j^\alpha\rangle\langle e_j^\alpha|$ as

$$V_p^\alpha \simeq \Omega_p e^{i\vec{k}_p \cdot \vec{r}} |e_1^\alpha\rangle\langle g^\alpha| + \text{H.c.}, \quad (2)$$

where $\vec{r}$ is the spatial location of the chiral molecule and Ω_p is the Rabi frequency corresponding to the transition $|g^\alpha\rangle \leftrightarrow |e_1^\alpha\rangle$ under the square pulse approximation. Note that the Hamiltonian presented in Eq. (2) is an approximate result, wherein we have neglected the interaction of the CTLS during the short duration of the probe pulses. This approximation is based on the assumption that the driving fields are significantly weaker than the probe pulses, i.e., $|\Omega_{jl}| \ll |\Omega_p|$.

In our previous work [27], a strict condition of one-photon resonance ($\Delta_{jl} = 0$) and a narrow-bandwidth probe-pulse assumption were considered. In this section, we release only the condition of one-photon resonance to show how the properties of the driving field impact the shape of the 2D spectra. We will show in Sec. III that pulses with a broad bandwidth could also be applied as probe pulses.

Starting from the initial state $|\psi_0^\alpha\rangle = |g^\alpha\rangle$ in the Schrödinger picture, the final state of the system after interaction with the sequence of the two pulses is

$$|\psi^\alpha(\tau, t)\rangle = U_{\text{cyc}}^\alpha(\tau + t + 2\delta t_p, \tau + 2\delta t_p) U_b^\alpha$$
$$\times U_{\text{cyc}}^\alpha(\tau + \delta t_p, \delta t_p) U_a^\alpha |\psi_0^\alpha\rangle, \quad (3)$$

where $U_p^\alpha = \exp[-iH_0^\alpha \delta t_p] \exp[-iV_p^\alpha \delta t_p]$ and $U_{\text{cyc}}^\alpha(s + s', s') = \exp[-iH'_\alpha(s + s')] \exp[-iV_{\text{cyc}}^\alpha s] \exp[iH'_\alpha s']$ are evolution operators inside and outside the pulse duration, respectively. We note that $U_{\text{cyc}}^\alpha(s + s', s')$ is the evolution operator in the Schrödinger picture, and a similar operator in Ref. [27] should be corrected but does not affect the main

result. The final polarization $\boldsymbol{P}^\alpha(\tau, t) \equiv \langle \psi^\alpha(\tau, t) | \hat{\boldsymbol{\mu}}^\alpha | \psi^\alpha(\tau, t) \rangle$ will yield signal fields along multiple phase-matching directions [44–46], and we sort only the rephasing signal that is emitted along $-\vec{k}_a + 2\vec{k}_b$.

In the final polarization, the rephasing part is calculated as $\boldsymbol{P}^\alpha_{\mathrm{RP}}(\tau, t) = \boldsymbol{A}^\alpha(\tau, t) e^{i(-\vec{k}_a + 2\vec{k}_b)\cdot\vec{r}}$. Here,

$$\boldsymbol{A}^\alpha(\tau, t) = \mathcal{N}_a^2 \mathcal{N}_b^2 \beta_a^* |\beta_b|^2 \sum_{j'} \left|n_{1j'}^\alpha\right|^2 e^{i(\omega_1' + E_{j'}^\alpha)\tau}$$

$$\times \sum_j \left|n_{1j}^\alpha\right|^2 e^{-i(\omega_1' + E_j^\alpha)t} \boldsymbol{\mu}_{01} \quad (4)$$

is the amplitude of the rephasing signal, $\hat{\boldsymbol{\mu}}^\alpha$ is the transition dipole operator, $\boldsymbol{\mu}_{01}^\alpha = \boldsymbol{\mu}_{01}$ is the transition dipole moment corresponding to the transition $|g^\alpha\rangle \leftrightarrow |e_1^\alpha\rangle$, $\beta_p = -i\Omega_p \delta t_p$ are transition amplitudes, $\mathcal{N}_p = (1 + |\beta_p|^2)^{-1/2}$ are normalized constants, $n_{lj} = \langle e_l^\alpha | d_j^\alpha \rangle$ are transformation-matrix elements, and $|d_j^\alpha\rangle$ and E_j^α are eigenvectors and eigenvalues of V_{cyc}^α. Adding the decoherence of the system during the whole process, the rephasing signal in Eq. (4) is modified as

$$\boldsymbol{A}^\alpha(\tau, t) = \mathcal{N}_a^2 \mathcal{N}_b^2 \beta_a^* |\beta_b|^2 \sum_{j'} \left|n_{1j'}^\alpha\right|^2 e^{i(\omega_1' + E_{j'}^\alpha)\tau} e^{-\Gamma\tau}$$

$$\times \sum_j \left|n_{1j}^\alpha\right|^2 e^{-i(\omega_1' + E_j^\alpha)t} e^{-\Gamma t} \boldsymbol{\mu}_{01}, \quad (5)$$

where $\Gamma = \gamma_{\mathrm{rl}}/2 + \gamma_{\mathrm{dp}}$ is the decoherence rate and γ_{rl} and γ_{dp} are, respectively, the relaxation and pure dephasing rates of the excited states.

For a mixture, the total signal from the two enantiomers is

$$\boldsymbol{A}^{\mathrm{mix}}(\tau, t) = N_L \boldsymbol{A}^L(\tau, t) + N_R \boldsymbol{A}^R(\tau, t), \quad (6)$$

where N_L and N_R are the numbers of left- and right-handed molecules in the mixture sample. The 2D spectrum

$$\tilde{\boldsymbol{A}}^{\mathrm{mix}}(\omega_\tau, \omega_t) \equiv \mathcal{F}[\boldsymbol{A}^{\mathrm{mix}}(\tau, t)] \quad (7)$$

is obtained by Fourier transforming [47] $\boldsymbol{A}^{\mathrm{mix}}(\tau, t)$ with respect to both the delay time τ and data-collecting time t.

We take the gaseous 1,2-propanediol, whose skeletal formula is shown in Fig. 2(a), as our example in this study and present a numerically simulated 2D spectrum of the racemic mixture (50:50 mixture of two enantiomers) in Fig. 2(c), which is zoomed in around $(\omega_1', -\omega_1')$. Neglecting the chirality index, the working states are chosen to be $|g\rangle = |v_g\rangle|0_{0,0,0}\rangle$, $|e_1\rangle = |v_e\rangle|1_{1,1,1}\rangle$, $|e_2\rangle = |v_e\rangle|2_{2,1,2}\rangle$, and $|e_3\rangle = |v_e\rangle|2_{2,0,1}\rangle$, where the vibrational ground (first-excited) state is denoted as $|v_g\rangle$ ($|v_e\rangle$) and the rotational states are denoted in the $|J_{K_a,K_c,M}\rangle$ notation [48]. With these working states, the transition frequencies are $\omega_{10}/2\pi \simeq 4.33$ THz, $\omega_{21}/2\pi \simeq 29.21$ GHz, $\omega_{31}/2\pi \simeq 29.31$ GHz, and $\omega_{32}/2\pi \simeq 100.76$ MHz [27,49,50]. The relaxation and pure dephasing rates are approximately taken as $\gamma_{\mathrm{rl}}/2\pi \simeq 1$ kHz and $\gamma_{\mathrm{dp}}/2\pi \simeq 0.1$ MHz [43,51]. The CTLS is assumed to have detunings $\Delta_{21}/2\pi = 1$ MHz and $\Delta_{31}/2\pi = 1.5$ MHz of the driving fields; Rabi frequencies $\Omega_{21}/2\pi = 4$ MHz, $\Omega_{31}/2\pi = 4$ MHz, and $\Omega_{32}/2\pi = 4.5$ MHz; and overall phases $\varphi^L = 2\pi/7$ and $\varphi^R = 9\pi/7$. The probe pulses have duration $\delta t_p \simeq 0.5$ ns with Fourier-limited bandwidth $\delta\nu \simeq 2\pi \times 1.8$ GHz $\ll \{\omega_{21}, \omega_{31}\}$ and corresponding Rabi frequencies
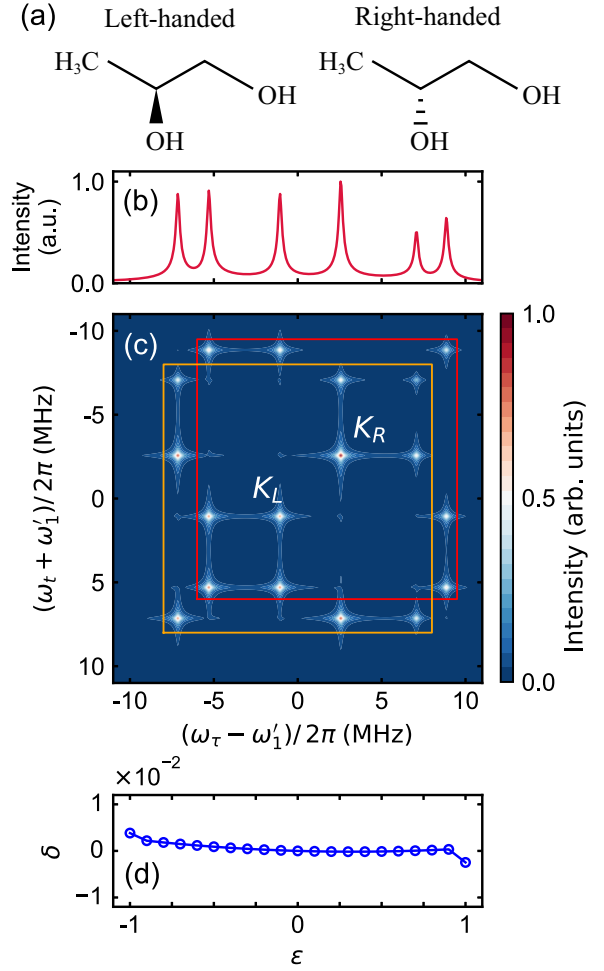

FIG. 2. (a) The skeletal formulas of two enantiomers of 1,2-propanediol, which is taken as an example. (b) The 1D and (c) 2D spectra of the racemic mixture (50:50 mixture of two enantiomers) of gaseous 1,2-propanediol. The 1D spectrum is the projection of the 2D spectrum on the axis of ω_τ. The 2D spectrum is obtained by taking only the absolute value of the Fourier transform. (c) K_L and K_R denote the amplitudes of the two strongest peaks that belong to left-handed and right-handed enantiomers, respectively. (d) The error $\delta = \varepsilon_e - \varepsilon$ between the enantiomeric excess ε_e estimated by the intensity ratio of the peaks denoted in (c) and the real value ε. The parameters for the simulation are chosen to be $\Omega_p/2\pi \simeq 100$ MHz, $\Omega_{21}/2\pi = 4$ MHz, $\Omega_{31}/2\pi = 4$ MHz, $\Omega_{32}/2\pi = 4.5$ MHz, $\Delta_{21}/2\pi = 1$ MHz, $\Delta_{31}/2\pi = 1.5$ MHz, $\gamma_{\mathrm{rl}}/2\pi \simeq 1$ kHz, $\gamma_{\mathrm{dp}}/2\pi \simeq 0.1$ MHz, $\varphi^L = 2\pi/7$, and $\varphi^R = 9\pi/7$.

$\Omega_p/2\pi \simeq 100$ MHz. The time-domain signal is scanned from 0 to 20 μs with a step size of 0.01 μs.

According to Eq. (5), each enantiomer has nine peaks in the 2D spectrum in Fig. 2(c) at locations $(\omega_1' + E_{j'}^\alpha, -\omega_1' - E_j^\alpha)$. Those nine peaks form a grouped pattern, with three diagonal peaks resulting in six off-diagonal ones. The lack of off-diagonal correspondence between any two diagonal peaks indicates that they belong to opposite chiralities. For instance, nine peaks enclosed by red lines in Fig. 2(c) share the same chirality (i.e., left-handed chirality), and the other nine peaks enclosed by orange lines share the opposite chirality (i.e., right-hand chirality). We note that such a direct categorization

is not possible within a single 1D spectrum [e.g., the one in Fig. 2(b)] without an additional procedure [26,29].

We remark that the distinct nine-peak pattern is the general case and different patterns with fewer than nine peaks may appear due to the degeneracy of E_j^α [27] or the inequality of $|n_{1j}^\alpha|^2$. Nevertheless, the chirality categorization can always be achieved by referring the off-diagonal peaks.

After the chirality categorization, the enantiomeric excess $\varepsilon = (N_L - N_R)/(N_L + N_R)$ of the chiral mixture is estimated using the intensity ratio of the peaks in the 2D spectrum. To clarify the notation used in our analysis, we denote the amplitudes of the two strongest diagonal peaks belonging to different enantiomers at locations $(\omega_L, -\omega_L)$ and $(\omega_R, -\omega_R)$ as K_L and K_R, where

$$K_\alpha = N_L|\tilde{A}^L(\omega_\alpha, -\omega_\alpha)| + N_R|\tilde{A}^R(\omega_\alpha, -\omega_\alpha)|, \qquad (8)$$

where $\omega_\alpha = \omega_1' + E_2^\alpha$, with $E_2^L/2\pi = -1.060\,\text{MHz}$ and $E_2^R/2\pi = 2.566\,\text{MHz}$. Since the peaks belonging to different enantiomers are well separated, the left-handed enantiomer makes very few contributions to K_R and vice versa, i.e., $|\tilde{A}^L(\omega_L, -\omega_L)| \gg |\tilde{A}^R(\omega_L, -\omega_L)|$, $|\tilde{A}^R(\omega_R, -\omega_R)| \gg |\tilde{A}^L(\omega_R, -\omega_R)|$, and

$$K_\alpha \simeq N_\alpha|\tilde{A}^\alpha(\omega_\alpha, -\omega_\alpha)|. \qquad (9)$$

In the one-photon resonance case ($\Delta_{jl} = 0$) of the CTLS, the enantiopure signal intensities are always equal, $|\tilde{A}^L(\omega_L, -\omega_L)| = |\tilde{A}^R(\omega_R, -\omega_R)|$, due to the equality of the absolute value [27] of the corresponding transformation-matrix elements $|n_{1j}^L| = |n_{1j}^R|$. The enantiomeric excess is estimated using the equation $\varepsilon_e = (K_L - K_R)/(K_L + K_R)$.

However, in the general three-photon resonance case $(\Delta_{21} + \Delta_{32} = \Delta_{31})$, the absolute values of the transformation-matrix elements are typically not equal and are often unknown beforehand. Therefore, we use the racemic mixture of chiral molecules, which is easily accessible and readily available, as the reference sample to obtain the parameter

$$\lambda = \frac{K_L^{\text{rm}}}{K_R^{\text{rm}}}, \qquad (10)$$

and the enantiomeric excess is estimated as

$$\varepsilon_e = \frac{K_L - \lambda K_R}{K_L + \lambda K_R}. \qquad (11)$$

We demonstrate the numerical estimation error $\delta = \varepsilon_e - \varepsilon$ as a function of ε in Fig. 2(d), and we observe that the absolute value of the error is consistently less than 0.5×10^{-2}.

In our previous work [27], three one-photon resonances (a special case of the three-photon resonance) of the CTLS were utilized. Such a condition demands that one know the energy levels of the investigated chiral molecule precisely and possesses three microwave fields with specific frequencies, which remains challenging for most molecules. When the energy levels of the chiral molecules are only roughly known, the three driving fields will typically couple to the corresponding transitions with slight detunings, breaking the one-photon resonance condition. In such a case, we demonstrated in this section that three-photon resonance of the CTLS can be

used and our method remains applicable for enantiodetection. Compared with the one-photon resonance condition, the three-photon resonance merely demands precise frequency control of the driving fields to satisfy the relation $\nu_{21} + \nu_{32} = \nu_{31}$, making it more easily attainable in experimental practice. In addition, we remark that three-photon resonance is a necessity in our method for the CTLS to yield consistent chirality-dependent energy shifts.

III. BROADBAND PROBE PULSE

In the above discussion, we have assumed that only one transition $|g^\alpha\rangle \leftrightarrow |e_1^\alpha\rangle$ is induced by the probe pulses with the narrow-band assumption. However, in experimental conditions, the pulse bandwidth is usually much broader, on the order of several terahertz [39–41], which means that all three transitions $|g^\alpha\rangle \leftrightarrow |e_j^\alpha\rangle$ may be induced (if the selection rule [32,34,35] permits). Despite the specifically chosen working states, some other redundant states can get involved in the probing process as noise.

We prove in this section that the chiral molecules are still distinguishable in the 2D spectrum even if more than one transition is induced by the probe pulses. Furthermore, the influence of other redundant states is eliminated by the chop-detection method, which is typically used in optical experiments [39–41].

A. Inducing transitions to multiple excited working states

Instead of the narrow-band assumption, we here and in the following assume that the bandwidth of the probe pulses is so broad that all transitions $|g^\alpha\rangle \leftrightarrow |e_j^\alpha\rangle$ are nearly resonantly induced [52]. Thus, the Hamiltonian of the system within the pulse duration is given in the interaction picture with respect to H_0^α as

$$V_{p,3\text{e}}^\alpha = \sum_j \Omega_{p,j}^\alpha e^{i\vec{k}_p \cdot \vec{r}} |e_j^\alpha\rangle\langle g^\alpha| + \text{H.c.}, \qquad (12)$$

and the rephasing signal is correspondingly modified as

$$\begin{aligned}
\boldsymbol{A}_{3\text{e}}^\alpha(\tau, t) = & \left[\mathcal{N}_{a,0}^\alpha\right]^2 \mathcal{N}_{b,0}^\alpha \sum_{m,m'} \left[\beta_{a,m}^\alpha\right]^* \beta_{b,m'}^\alpha \\
& \times \sum_{j,l} \left[n_{lj}^\alpha\right]^* n_{mj}^\alpha \mathcal{N}_{b,l}^\alpha \left[\beta_{b,l}^\alpha\right]^* \\
& \times \sum_{j',l'} n_{l'j'}^\alpha \left[n_{m'j'}^\alpha\right]^* e^{-i(\omega_{l'}' + E_j^\alpha)t} e^{-\Gamma t} \\
& \times e^{i(\omega_l' + \omega_{m'}' - \omega_{l'}' + E_j^\alpha)\tau} e^{-\Gamma \tau} \boldsymbol{\mu}_{0l'}^\alpha. \qquad (13)
\end{aligned}$$

Here, $\boldsymbol{\mu}_{0j}^\alpha$ and $\Omega_{p,j}^\alpha$ are transition dipole moments and Rabi frequencies corresponding to transitions $|g^\alpha\rangle \leftrightarrow |e_j^\alpha\rangle$, $\beta_{p,j}^\alpha = -i\Omega_{p,j}^\alpha \delta t_p$ are transition amplitudes, and $\mathcal{N}_{p,j}^\alpha = (1 + |\beta_{p,j}^\alpha|^2)^{-1/2}$ and $\mathcal{N}_{p,0}^\alpha = (1 + \sum_j |\beta_{p,j}^\alpha|^2)^{-1/2}$ are normalized constants. We specify the transition dipole moments as $\boldsymbol{\mu}_{01}^L = \boldsymbol{\mu}_{01}^R = \boldsymbol{\mu}_{01}$, $\boldsymbol{\mu}_{02}^L = -\boldsymbol{\mu}_{02}^R = \boldsymbol{\mu}_{02}$, and $\boldsymbol{\mu}_{03}^L = -\boldsymbol{\mu}_{03}^R = \boldsymbol{\mu}_{03}$ to fulfill the cyclic conditions of the new cyclic structures formed by levels $|g^\alpha\rangle$, $|e_j^\alpha\rangle$, and $|e_{j'}^\alpha\rangle$ ($j \neq j'$). For the special case with the selection rule considered, one or two of the transitions $|g^\alpha\rangle \leftrightarrow |e_j^\alpha\rangle$ may be forbidden, i.e., $\boldsymbol{\mu}_{0j} = 0$. Especially, when two of the three transitions are forbidden, the rephasing signal
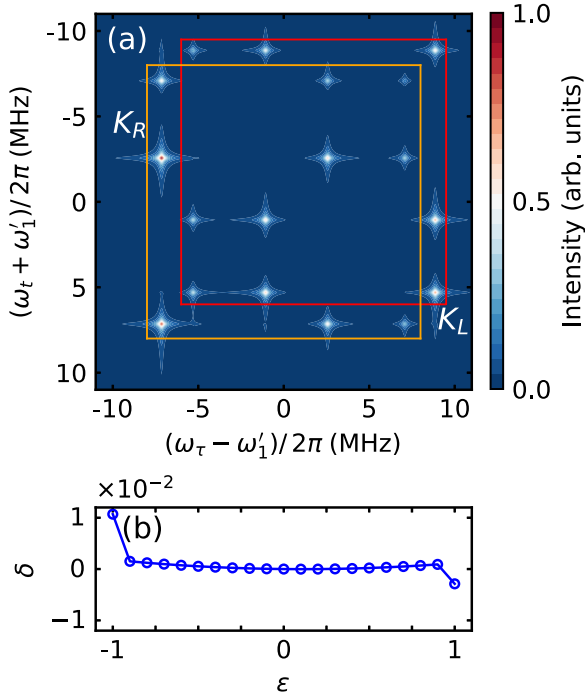
FIG. 3. (a) The 2D spectrum of the racemic mixture of gaseous 1,2-propanediol when both transitions $|g^\alpha\rangle \leftrightarrow |e_1^\alpha\rangle$ and $|g^\alpha\rangle \leftrightarrow |e_2^\alpha\rangle$ are induced by the probe pulses. (b) The error of the estimation of the enantiomeric excess estimated by the intensity ratio of the peaks denoted in (a). In the simulation, the Rabi frequencies between the ground state and the excited states are chosen to be $\Omega_{p,1}^L = \Omega_{p,1}^R = 2\pi \times 100$ MHz and $\Omega_{p,2}^L = -\Omega_{p,2}^R = 2\pi \times 100$ MHz, and the transition $|g^\alpha\rangle \leftrightarrow |e_3^\alpha\rangle$ is forbidden. The other parameters are the same as those in Fig. 2.

in Eq. (13) retains the one in Eq. (5) where only one transition is considered. We note that the phases accumulated during the pulse interaction are neglected in Eq. (13) because of the short duration of the pulses (see the Appendix for detailed result).

The 2D spectrum is obtained by Fourier transforming $A_{3e}^\alpha(\tau, t)$ with respect to τ and t. We still zoom in around $(\omega_1', -\omega_1')$, where the peaks correspond to terms with $\{l, l', m'\} = 1$ in Eq. (13). The phase factors containing τ and t of such terms are exactly the same as those in Eq. (5). Thus, the peaks still locate at positions $(\omega_1' + E_{j'}^\alpha, -\omega_1' - E_j^\alpha)$ even though broadband probe pulses are applied. However, the peak amplitudes change due to the different interaction.

The simulated 2D spectrum of the racemic mixture with two transitions $|g^\alpha\rangle \leftrightarrow |e_1^\alpha\rangle$ and $|g^\alpha\rangle \leftrightarrow |e_2^\alpha\rangle$ induced is presented in Fig. 3(a) by taking the working states of 1,2-propanediol as $|g\rangle = |v_g\rangle|0_{0,0,0}\rangle$, $|e_1\rangle = |v_e\rangle|1_{1,1,1}\rangle$, $|e_2\rangle = |v_e\rangle|1_{1,0,1}\rangle$, and $|e_3\rangle = |v_e\rangle|2_{2,0,1}\rangle$.

The transition frequencies in the CTLS are $\omega_{21}/2\pi \simeq 846.79$ MHz, $\omega_{31}/2\pi \simeq 29.31$ GHz, and $\omega_{32}/2\pi \simeq 28.46$ GHz [49,50]. We maintain the same assumptions regarding the detunings, Rabi frequencies, and overall phases of the CTLS as described in Sec. II. However, we modify the assumption of the probe pulses to have a bandwidth of $\delta\nu/2\pi \simeq 0.9$ THz (with duration $\delta t_p \simeq 1$ ps) and central frequency of $\nu_p/2\pi \simeq 4.33$ THz. With such a broad bandwidth, all three transitions $|g^\alpha\rangle \leftrightarrow |e_j^\alpha\rangle$ are covered, but the

transition $|g^\alpha\rangle \leftrightarrow |e_3^\alpha\rangle$ is forbidden since $\Delta J = 2$ [32,34,35]. Moreover, we take $\Omega_{p,1}^L = \Omega_{p,1}^R = 2\pi \times 100$ MHz and $\Omega_{p,2}^L = -\Omega_{p,2}^R = 2\pi \times 100$ MHz.

To determine the enantiomeric excess, we also denote the amplitudes of the two strongest diagonal peaks belonging to different enantiomers as K_L and K_R in Fig. 3(a). These two peaks locate at $(\omega_L', -\omega_L')$ and $(\omega_R', -\omega_R')$, respectively, where $\omega_L' = \omega_1' + E_3^L$ and $\omega_R' = \omega_1' + E_1^R$, with $E_3^L/2\pi = 8.861$ MHz and $E_1^R/2\pi = -7.145$ MHz. The estimation of enantiomeric excess is obtained using Eq. (11) by taking the racemic mixture as the reference. Figure 3(b) shows that the errors of such estimation are still well below 1×10^{-2} in most regions even with broadband probe pulses.

B. Inducing transitions to redundant excited states

Apart from the chosen working states, real chiral molecules have complex rotational levels [41], which will yield massive redundant peaks on the 2D spectrum, disturbing the categorization of the chirality of the peaks. For the case in Sec. III A, the transition between the ground state and a redundant excited state $|e_{rd}\rangle = |v_e\rangle|1_{0,1,1}\rangle$ could also be induced by the probe pulses. Such a state will not introduce an additional cyclic loop since the transition frequencies between $|e_{rd}\rangle$ and $|e_j^\alpha\rangle$ ($2\pi \times 4.89$ GHz, $2\pi \times 5.74$ GHz, and $2\pi \times 34.20$ GHz) are all significantly nonresonant with the frequencies of the driving fields. We take into account this redundant state and modify the Hamiltonian within the pulse duration in the interaction picture with respect to H_0^α as $V_{p,me}^\alpha = V_{p,3e}^\alpha + V_{rd}^\alpha$, where

$$V_{rd}^\alpha = \Omega_{p,rd} e^{i\vec{k}_p \cdot \vec{r}} |e_{rd}^\alpha\rangle\langle g^\alpha| + \text{H.c.} \qquad (14)$$

and $\Omega_{p,rd}$ is the Rabi frequency corresponding to the transition $|g^\alpha\rangle \leftrightarrow |e_{rd}^\alpha\rangle$. Given this Hamiltonian, the final rephasing signal is $A_{me}^\alpha = A_{3e}^\alpha + A_{rd1}^\alpha + A_{rd2}^\alpha$, with

$$A_{rd1}^\alpha(\tau, t) = [\mathcal{N}_{a,0}^\alpha]^2 \mathcal{N}_{b,0}^\alpha \mathcal{N}_{b,rd} \beta_{a,rd}^* |\beta_{b,rd}|^2 e^{i\omega_{rd}\tau} e^{-\Gamma\tau}$$
$$\times e^{-i\omega_{rd}t} e^{-\Gamma t} \boldsymbol{\mu}_{rd} \qquad (15)$$

and

$$A_{rd2}^\alpha(\tau, t) = [\mathcal{N}_{a,0}^\alpha]^2 \mathcal{N}_{b,0}^\alpha \mathcal{N}_{b,rd} [\beta_{a,rd} \beta_{b,rd}]^*$$
$$\times \sum_m \beta_{b,m}^\alpha \sum_{j,l} n_{lj}^\alpha [n_{mj}^\alpha]^* e^{-i(\omega_l' + E_j^\alpha)t} e^{-\Gamma t}$$
$$\times e^{i(\omega_{rd} + \omega_m' - \omega_l')\tau} e^{-\Gamma\tau} \boldsymbol{\mu}_{0l}^\alpha$$
$$+ [\mathcal{N}_{a,0}^\alpha]^2 \mathcal{N}_{b,0}^\alpha \beta_{b,rd} \sum_m [\beta_{a,m}^\alpha]^* \sum_{j,l} \mathcal{N}_{b,l}^\alpha [\beta_{b,l}^\alpha]^*$$
$$\times [n_{lj}^\alpha]^* n_{mj}^\alpha e^{i(\omega_l' + E_j^\alpha)\tau} e^{-\Gamma\tau} e^{-i\omega_{rd}t} e^{-\Gamma t} \boldsymbol{\mu}_{rd}, \quad (16)$$

where ω_{rd} is the eigenenergy of the redundant level $|e_{rd}^\alpha\rangle$; $\beta_{p,rd} = -i\Omega_{p,rd}\delta t_p$ is the transition amplitude; $\mathcal{N}_{p,j}^\alpha = (1 + |\beta_{p,j}^\alpha|^2)^{-1/2}$, $\mathcal{N}_{p,rd} = (1 + |\beta_{p,rd}|^2)^{-1/2}$, and $\mathcal{N}_{p,0}^\alpha = (1 + |\beta_{p,rd}|^2 + \sum_j |\beta_{p,j}^\alpha|^2)^{-1/2}$ are the normalized constants; and $\boldsymbol{\mu}_{rd}^\alpha = \boldsymbol{\mu}_{rd}$ is the transition dipole moment corresponding to the transition $|g^\alpha\rangle \leftrightarrow |e_{rd}^\alpha\rangle$.

According to $A_{rd1}^\alpha(\tau, t)$ in Eq. (15), there is an additional diagonal peak at location $(\omega_{rd}, -\omega_{rd})$ in the Fourier-transformed 2D spectrum. This peak has no chiral feature
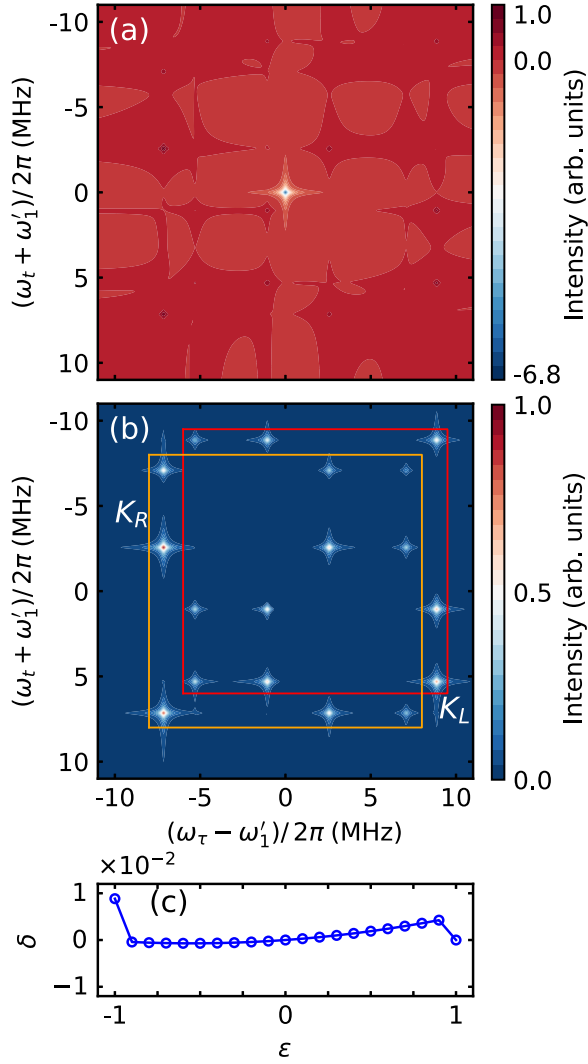
FIG. 4. (a) Chop-detected 2D spectrum of the racemic mixture of gaseous 1,2-propanediol. The deep negative peak at the center corresponds to the free eigenstate $|e_1^\alpha\rangle$ of 1,2-propanediol. (b) The truncated 2D spectrum of (a) neglecting all the negative values. (c) The error of the estimated enantiomeric excess with chop detection and truncation. For the simulation, the parameters here are taken to be the same as those in Fig. 3.

$(\mathcal{N}_{p,0}^L = \mathcal{N}_{p,0}^R)$ and is not affected by the driving fields in the CTLS. We thus eliminate it through chop detection [39–41] by conducting two experiments with driving fields on and off. The chop-detected signal is given in the frequency domain as

$$\tilde{A}_{\text{chop}}^\alpha(\omega_\tau, \omega_t) = \left| \tilde{A}_{3\text{e,on}}^\alpha(\omega_\tau, \omega_t) \right| - \left| \tilde{A}_{3\text{e,off}}^\alpha(\omega_\tau, \omega_t) \right|$$
$$+ \left| \tilde{A}_{\text{rd2,on}}^\alpha(\omega_\tau, \omega_t) \right| - \left| \tilde{A}_{\text{rd2,off}}^\alpha(\omega_\tau, \omega_t) \right|. \tag{17}$$

The two terms $|\tilde{A}_{\text{rd2,on}}^\alpha(\omega_\tau, \omega_t)|$ and $|\tilde{A}_{\text{rd2,off}}^\alpha(\omega_\tau, \omega_t)|$ have only off-diagonal peaks and thus would not disturb the chirality categorization of the diagonal peaks.

Figure 4(a) shows the chop-detected 2D spectrum of the racemic mixture. On the spectrum, a deep negative peak

is located at $(\omega_1', -\omega_1')$. This negative peak corresponds to the subtraction of $|\tilde{A}_{3\text{e,off}}^\alpha(\omega_\tau, \omega_t)|$ and strongly overshadows other chirality-dependent peaks. To eliminate its disturbance, we make a truncation in $\tilde{A}_{\text{chop}}^\alpha(\omega_\tau, \omega_t)$ by neglecting all the negative values, and the result is presented in Fig. 4(b). The truncated spectrum is almost the same as the one in Fig. 3(a) and still gives good estimations of the enantiomeric excess with sufficiently low errors, e.g., those below 1×10^{-2} in Fig. 4(c).

IV. SUMMARY AND DISCUSSION

This study has successfully demonstrated the effectiveness of the enantiodetection method via 2D spectroscopy [27] under more general experimental conditions. The previous method [27] was proposed with a strict condition of one-photon resonance in the CTLS and a narrowband probe-pulse assumption, limiting its applicability. However, in this study, we have shown that even with three-photon resonance in the CTLS and broadband probe pulses, different enantiomers can still produce chirality-dependent peaks in the 2D spectrum. It is important to note that identifying the chirality categorization of the peaks is not possible in the 1D spectrum without further information. Therefore, this method provides a significant advantage over traditional techniques. Additionally, we have found that the peak intensities for different enantiomers are not equal due to the inequality of the transformation matrix under three-photon resonance. Therefore, the enantiomeric excess of the chiral mixture is estimated using the racemic mixture as the reference.

Besides the advantage of distinguishing the chiral signal, our method also presents adequate accuracy for determining the enantiomeric excess. We have shown with numerical simulation that the error in our estimation of the enantiomeric excess is typically below 0.01, comparable to what has been reported in three-wave mixing approaches [22,23], e.g., 0.025 ± 0.005 for a chiral mixture of gaseous 1,2-propanediol with a known 0.02 enantiomeric excess [23].

Real systems of chiral molecules contain massive redundant levels that can disturb the chirality categorization. To eliminate this disturbance, we have implemented chop detection and truncation. These methods have proven to be effective in reducing the influence of redundant levels and ensuring accurate enantiodetection results.

Overall, this study has provided valuable insights into the effectiveness of the enantiodetection method via 2D spectroscopy and its applicability under more general experimental conditions.

APPENDIX: CALCULATION OF THE FINAL STATE AND POLARIZATION WITHOUT A REDUNDANT STATE

In this Appendix, we calculate the final state and polarization of the system under three-photon resonance with broadband probe pulses inducing all three working transitions $|g^\alpha\rangle \leftrightarrow |e_j^\alpha\rangle$.

For initial state $|g^\alpha\rangle$ or $|e_l^\alpha\rangle$ at time s' of the system, the evolved states after an evolution time s without the probe pulses are given in the Schrödinger picture as

$$U_{\text{cyc}}^\alpha(s + s', s')|g^\alpha\rangle = |g^\alpha\rangle, \tag{A1}$$

$$U_{\text{cyc}}^\alpha(s + s', s')\big|e_l^\alpha\big\rangle = \sum_{j,j'} n_{j'j}^\alpha \big[n_{lj}^\alpha\big]^* e^{-iE_j^\alpha s} e^{-i\omega_{j'}'(s + s')} e^{i\omega_l' s'}\big|e_{j'}^\alpha\big\rangle, \tag{A2}$$

where $U_{\text{cyc}}^\alpha(s + s', s') = \exp[-iH_\alpha'(s + s')]\exp[-iV_{\text{cyc}}^\alpha s]\exp[iH_\alpha' s']$ is the evolution operator outside the pulse duration.

On the other hand, the evolved states after the whole pulse duration are given in the Schrödinger picture as

$$U_{p,3e}^\alpha|g^\alpha\rangle = \cos\big(\Omega_{p,3e}^\alpha \delta t_p\big)|g^\alpha\rangle - i\sin\big(\Omega_{p,3e}^\alpha \delta t_p\big)e^{i\vec{k}_p\cdot\vec{r}} \sum_j \frac{\Omega_{p,j}^\alpha}{\Omega_{p,3e}^\alpha} e^{-i\omega_j \delta t_p}\big|e_j^\alpha\big\rangle, \tag{A3}$$

$$U_{p,3e}^\alpha\big|e_j^\alpha\big\rangle = -i\frac{\Omega_{p,j}^\alpha}{\Omega_{p,3e}^\alpha}\sin\big(\Omega_{p,3e}^\alpha \delta t_p\big)e^{-i\vec{k}_p\cdot\vec{r}}|g^\alpha\rangle + \left[1 - \left(\frac{\Omega_{p,j}^\alpha}{\Omega_{p,3e}^\alpha}\right)^2\big[1 - \cos\big(\Omega_{p,3e}^\alpha \delta t_p\big)\big]\right]e^{-i\omega_j \delta t_p}\big|e_j^\alpha\big\rangle$$

$$+ \sum_{l\neq j}\left[-\frac{\Omega_{p,j}^\alpha \Omega_{p,l}^\alpha}{\big(\Omega_{p,3e}^\alpha\big)^2}\big[1 - \cos\big(\Omega_{p,3e}^\alpha \delta t_p\big)\big]\right]e^{-i\omega_l \delta t_p}\big|e_l^\alpha\big\rangle, \tag{A4}$$

where $\Omega_{p,3e}^\alpha = \sqrt{\Omega_{p,1}^2 + \Omega_{p,2}^2 + \Omega_{p,3}^2}$ and $U_{p,3e}^\alpha = \exp[-iH_0^\alpha \delta t_p]\exp[-iV_{p,3e}^\alpha \delta t_p]$ is the evolution operator within the pulse duration. In the perturbative regime, i.e., $|\Omega_{p,3e}^\alpha \delta t_p| \ll 1$, the evolved states are approximately

$$U_{p,3e}^\alpha|g^\alpha\rangle = \mathcal{N}_{p,0}^\alpha\left(|g^\alpha\rangle + e^{i\vec{k}_p\cdot\vec{r}}\sum_j \beta_{p,j}^\alpha e^{-i\omega_j \delta t_p}\big|e_j^\alpha\big\rangle\right), \tag{A5}$$

$$U_{p,3e}^\alpha\big|e_j^\alpha\big\rangle = \mathcal{N}_{p,j}^\alpha\left(\big|e_j^\alpha\big\rangle + e^{-i\vec{k}_p\cdot\vec{r}}\beta_{p,j}^\alpha e^{-i\omega_j \delta t_p}|g^\alpha\rangle\right). \tag{A6}$$

Here, $\beta_{p,j}^\alpha = -i\Omega_{p,j}^\alpha \delta t_p$ are transition amplitudes, and $\mathcal{N}_{p,j}^\alpha = (1 + |\beta_{p,j}^\alpha|^2)^{-1/2}$ and $\mathcal{N}_{p,0}^\alpha = (1 + \sum_j |\beta_{p,j}^\alpha|^2)^{-1/2}$ are normalized constants.

In our proposed experiment with the sequence of two probe pulses, the final state of the system with initial state $|\psi_0^\alpha\rangle = |g^\alpha\rangle$ is calculated as

$$\big|\psi_{3e}^\alpha(\tau, t)\big\rangle = U_{\text{cyc}}^\alpha(\tau + t + 2\delta t_p, \tau + 2\delta t_p)U_b^\alpha U_{\text{cyc}}^\alpha(\tau + \delta t_p, \delta t_p)U_a^\alpha\big|\psi_0^\alpha\big\rangle$$

$$= \mathcal{N}_{a,0}^\alpha \mathcal{N}_{b,0}^\alpha e^{i\vec{k}_b\cdot\vec{r}}\sum_m \beta_{b,m}^\alpha e^{-i\omega_m \delta t_p}\sum_{j,l} n_{lj}^\alpha\big[n_{mj}^\alpha\big]^* e^{-iE_j^\alpha t}e^{-i\omega_l'(\tau + t + 2\delta t_p)}e^{i\omega_m'(\tau + 2\delta t_p)}\big|e_l^\alpha\big\rangle$$

$$+ \mathcal{N}_{a,0}^\alpha e^{i(\vec{k}_a - \vec{k}_b)\cdot\vec{r}}\sum_m \beta_{a,m}^\alpha e^{-i\omega_m \delta t_p}\sum_{j,l} n_{lj}^\alpha\big[n_{mj}^\alpha\big]^* e^{-iE_j^\alpha \tau}e^{-i\omega_l'(\tau + \delta t_p)}e^{i\omega_m' \delta t_p}\mathcal{N}_{b,l}^\alpha \beta_{b,l}^\alpha|g^\alpha\rangle$$

$$+ \mathcal{N}_{a,0}^\alpha e^{i\vec{k}_a\cdot\vec{r}}\sum_m \beta_{a,m}^\alpha e^{-i\omega_m \delta t_p}\sum_{j,l} n_{lj}^\alpha\big[n_{mj}^\alpha\big]^* e^{-iE_j^\alpha \tau}e^{-i\omega_l'(\tau + \delta t_p)}e^{i\omega_m' \delta t_p}\mathcal{N}_{b,l}^\alpha e^{-i\omega_l \delta t_p}$$

$$\times \sum_{j',l'} n_{l'j'}^\alpha\big[n_{lj'}^\alpha\big]^* e^{-iE_{j'}^\alpha t}e^{-i\omega_{l'}'(\tau + t + 2\delta t_p)}e^{i\omega_l'(\tau + 2\delta t_p)}\big|e_{l'}^\alpha\big\rangle + \mathcal{N}_{a,0}^\alpha \mathcal{N}_{b,0}^\alpha|g^\alpha\rangle. \tag{A7}$$

With the final state, the polarization after the delay time τ and data-collecting time t is given by $\boldsymbol{P}_{3e}^\alpha(\tau, t) = \langle\psi_{3e}^\alpha(\tau, t)|\hat{\boldsymbol{\mu}}^\alpha|\psi_{3e}^\alpha(\tau, t)\rangle$. Adding the decoherence during τ and t, the amplitude of the rephasing part of the final polarization with phase factor $e^{i(-\vec{k}_a + 2\vec{k}_b)\cdot\vec{r}}$ is

$$\boldsymbol{A}_{3e}^\alpha(\tau, t) = \big[\mathcal{N}_{a,0}^\alpha\big]^2 \mathcal{N}_{b,0}^\alpha \sum_{m,m'}\big[\beta_{a,m}^\alpha\big]^* \beta_{b,m'}^\alpha e^{i(\omega_m - \omega_{m'})\delta t_p}\sum_{j,l}\big[n_{lj}^\alpha\big]^* n_{mj}^\alpha e^{i(\omega_l' - \omega_m')\delta t_p}\mathcal{N}_{b,l}^\alpha\big[\beta_{b,l}^\alpha\big]^*$$

$$\times \sum_{j',l'} n_{l'j'}^\alpha\big[n_{m'j'}^\alpha\big]^* e^{-i(\omega_{l'}' + E_{j'}^\alpha)t}e^{-\Gamma t}e^{i(\omega_l' + \omega_{m'}' - \omega_{l'}' + E_j^\alpha)\tau}e^{-\Gamma \tau}e^{2i(\omega_{m'}' - \omega_{l'}')\delta t_p}\boldsymbol{\mu}_{0l'}^\alpha. \tag{A8}$$

The result here is similar to Eq. (13), except that the phase factors $\exp[i(\omega_i - \omega_j)\delta t_p]$ and $\exp[i(\omega'_i - \omega'_j)\delta t_p]$ are neglected there because the pulse duration is typically so short that $\{|(\omega_i - \omega_j)\delta t_p|,\ |(\omega'_i - \omega'_j)\delta t_p|\} \ll 1$. Letting $\boldsymbol{\mu}^\alpha_{02}$ and $\boldsymbol{\mu}^\alpha_{03}$ be zero (i.e., only the transition $|g^\alpha\rangle \leftrightarrow |e^\alpha_1\rangle$ can be induced by the probe pulses), Eq. (A8) thus matches Eq. (5).

[1] M. Quack, Angew. Chem., Int. Ed. Engl. **28**, 571 (1989).

[2] A. Salam and W. J. Meath, J. Chem. Phys. **106**, 7865 (1997).

[3] A. Salam and W. Meath, Chem. Phys. **228**, 115 (1998).

[4] Y. Ma and A. Salam, Chem. Phys. **324**, 367 (2006).

[5] Y. Li, C. Bruder, and C. P. Sun, Phys. Rev. Lett. **99**, 130403 (2007).

[6] Y. Li and C. Bruder, Phys. Rev. A **77**, 015403 (2008).

[7] X. Li and M. Shapiro, J. Chem. Phys. **132**, 194315 (2010).

[8] F. Suzuki, T. Momose, and S. Y. Buhmann, Phys. Rev. A **99**, 012513 (2019).

[9] B. Liu, C. Ye, C. P. Sun, and Y. Li, Phys. Rev. A **104**, 013113 (2021).

[10] J. H. Lee, J. Bischoff, A. O. Hernandez-Castillo, B. Sartakov, G. Meijer, and S. Eibenberger-Arias, Phys. Rev. Lett. **128**, 173001 (2022).

[11] J. Shao and P. Hänggi, J. Chem. Phys. **107**, 9935 (1997).

[12] M. Shapiro, E. Frishman, and P. Brumer, Phys. Rev. Lett. **84**, 1669 (2000).

[13] K. Hoki, L. González, and Y. Fujimura, J. Chem. Phys. **116**, 8799 (2002).

[14] P. Král, I. Thanopulos, M. Shapiro, and D. Cohen, Phys. Rev. Lett. **90**, 033001 (2003).

[15] C. Ye, Y.-Y. Chen, Q. Zhang, and Y. Li, J. Phys. B **54**, 145102 (2021).

[16] C. Ye, B. Liu, Y.-Y. Chen, and Y. Li, Phys. Rev. A **103**, 022830 (2021).

[17] Y. He, B. Wang, R. K. Dukor, and L. A. Nafie, Appl. Spectrosc. **65**, 699 (2011).

[18] P. J. Stephens, J. Phys. Chem. **89**, 748 (1985).

[19] T. K. Begzjav, Z. Zhang, M. O. Scully, and G. S. Agarwal, Opt. Express **27**, 13965 (2019).

[20] M. M. R. Fanood, N. B. Ram, C. S. Lehmann, I. Powis, and M. H. M. Janssen, Nat. Commun. **6**, 7511 (2015).

[21] A. Ghosh and P. Fischer, Phys. Rev. Lett. **97**, 173002 (2006).

[22] D. Patterson, M. Schnell, and J. M. Doyle, Nature (London) **497**, 475 (2013).

[23] D. Patterson and J. M. Doyle, Phys. Rev. Lett. **111**, 023008 (2013).

[24] S. Lobsiger, C. Perez, L. Evangelisti, K. K. Lehmann, and B. H. Pate, J. Phys. Chem. Lett. **6**, 196 (2015).

[25] V. A. Shubert, D. Schmitz, C. Pérez, C. Medcraft, A. Krin, S. R. Domingos, D. Patterson, and M. Schnell, J. Phys. Chem. Lett. **7**, 341 (2016).

[26] C. Ye, Q. Zhang, Y.-Y. Chen, and Y. Li, Phys. Rev. A **100**, 033411 (2019).

[27] M.-R. Cai, C. Ye, H. Dong, and Y. Li, Phys. Rev. Lett. **129**, 103201 (2022).

[28] C. Ye, Y. Sun, Y. Li, and X. Zhang, J. Phys. Chem. Lett. **14**, 6772 (2023).

[29] W. Z. Jia and L. F. Wei, Phys. Rev. A **84**, 053849 (2011).

[30] C. Ye, Y. Sun, and X. Zhang, J. Phys. Chem. Lett. **12**, 8591 (2021).

[31] P. Král and M. Shapiro, Phys. Rev. Lett. **87**, 183002 (2001).

[32] A. Jacob and K. Hornberger, J. Chem. Phys. **137**, 044313 (2012).

[33] K. K. Lehmann, J. Chem. Phys. **149**, 094201 (2018).

[34] C. Ye, Q. Zhang, and Y. Li, Phys. Rev. A **98**, 063401 (2018).

[35] M. Leibscher, T. F. Giesen, and C. P. Koch, J. Chem. Phys. **151**, 014302 (2019).

[36] Q. Zhang, Y.-Y. Chen, C. Ye, and Y. Li, J. Phys. B **53**, 235103 (2020).

[37] D. M. Jonas, Science **300**, 1515 (2003).

[38] N. V. Vitanov and M. Drewsen, Phys. Rev. Lett. **122**, 173202 (2019).

[39] K. Reimann, M. Woerner, and T. Elsaesser, J. Chem. Phys. **154**, 120901 (2021).

[40] M. Woerner, W. Kuehn, P. Bowlan, K. Reimann, and T. Elsaesser, New J. Phys. **15**, 025039 (2013).

[41] J. Lu, Y. Zhang, H. Y. Hwang, B. K. Ofori-Okai, S. Fleischer, and K. A. Nelson, Proc. Natl. Acad. Sci. USA **113**, 11800 (2016).

[42] Y.-Y. Chen, C. Ye, Q. Zhang, and Y. Li, J. Chem. Phys. **152**, 204305 (2020).

[43] S. Eibenberger, J. Doyle, and D. Patterson, Phys. Rev. Lett. **118**, 123002 (2017).

[44] S. Mukamel, *Principles of Nonlinear Optical Spectroscopy*, Oxford Series in Optical and Imaging Sciences (Oxford University Press, Oxford, 1995).

[45] M. Cho, *Two-Dimensional Optical Spectroscopy* (CRC Press, Boca Raton, FL, 2009).

[46] P. Tian, D. Keusters, Y. Suzaki, and W. S. Warren, Science **300**, 1553 (2003).

[47] G. S. Schlau-Cohen, A. Ishizaki, and G. R. Fleming, Chem. Phys. **386**, 1 (2011).

[48] R. N. Zare, *Angular Momentum: Understanding Spatial Aspects in Chemistry and Physics* (Wiley, New York, 1988).

[49] F. Lovas, D. Plusquellic, B. H. Pate, J. L. Neill, M. T. Muckle, and A. J. Remijan, J. Mol. Spectrosc. **257**, 82 (2009).

[50] B. E. Arenas, S. Gruet, A. L. Steber, and M. Schnell, J. Mol. Spectrosc. **337**, 9 (2017).

[51] D. Patterson and J. M. Doyle, Mol. Phys. **110**, 1757 (2012).

[52] X. Zhang and H. Dong, Phys. Rev. A **106**, 043516 (2022).